PHYSICAL REVIEW B VOLUME 12, NUMBER 11 1 DECEMBER 1975

Flux distribution calculations in planar channeling

J. A. Ellison
University of New Mexico, Albuquerque, New Mexico 87131
(Received 24 February 1975)

A technique has been developed to calculate the spatial and velocity distributions of channeled ions in planar channeling as a function of the depth in a crystal. The continuum plane approximation is assumed but no assumptions about statistical equilibrium are made. At fixed depths, the distributions are found to exhibit both jump discontinuities and infinities, so an integral of the distributions over small intervals around various positions across the channel is calculated. Also, the distributions are found to change considerably with depth and the integrals as a function of depth give a clear picture of the flux-peaking phenomenon. The key idea in this technique is an examination of the motion of the ions in the phase plane; this turns out to be a very systematic way of ordering the particles and thereby gaining insight into the structure of the distributions. The technique is illustrated by examining the evolution of the spatial distribution with depth for channeling of 1-MeV helium ions along the {110} planes of silicon.

I. INTRODUCTION

Ion channeling has been an active area of both theoretical and experimental research over the past 10–15 years. Much of the basic theory of the channeling process can be found in a classic paper published by Lindhard[1] in 1965. The channeling effect has recently been comprehensively reviewed by Gemmell.[2] In addition, a recent book edited by Morgan[3] on channeling gives a detailed treatment both of the theory and application of ion channeling.

A problem of considerable current interest in planar (and axial) channeling is the calculation of the spatial and velocity distributions of channeled particles as they move through a crystal. The solution of this problem would give a better understanding of the channeling phenomenon. Recent experimental work[4] shows that in planar channeling there are significant oscillations in the minimum yield as a function of depth. Experiments in axial channeling[5] show that the particle density at the center of a channel oscillates with depth into the crystal. Also experiments with very thin crystals[2] show that patterns of transmitted particles are quite complex. These experiments illustrate that the spatial distribution is changing rapidly with depth. In addition, channeling techniques are widely used in locating impurity atoms in metals and semiconductors[6–8]; an understanding of the spatial distribution and its variation with depth is of central importance in these applications.

In this study we present a technique for calculating the spatial and velocity distributions of channeled particles at various depths into the crystal within the framework of the planar continuum model. No assumption of statistical equilibrium is made in this model. However, effects of thermal vibration of the lattice atoms and electron multiple scattering are not incorporated in the present model. The motion of the particles in the phase plane is introduced as a systematic way of ordering the particles and thereby gaining insight into the structure of the distributions. The motion of these particles is determined by numerically solving the differential equations of the continuum model.

Much of the previous work done in calculating spatial distributions has assumed statistical equilibrium. However there are exceptions. The Monte Carlo work of Barrett[9,10] has contributed significantly to the understanding of various depth effects in channeling such as the oscillations in minimum yield; these depth effects are closely related to the evolution of the spatial and velocity distributions. Van Vliet[11] and Morgan and Van Vliet[12] have used computer simulation[13] to study the spatial distributions in axial channeling; they discuss the depth dependence of the particle density at various positions in the transverse plane both with and without multiple scattering effects. This differs from the present approach in that they used computer simulation and we use an analytical approach that does not assume statistical equilibrium. In addition very little computer simulation work has been done in planar channeling. An abstract of recent work by Abel *et al.*[4] indicates they have done some spatial-distribution calculations in planar channeling in which they also begin with the differential equations of motion in the continuum model.

We begin by discussing the equations of motion for an ion channeled between two crystal planes; these are well-known equations for a nonlinear oscillator. Then we illustrate how the phase plane can be used to develop an algorithm for computing the spatial and velocity distributions at various crystal depths. These distributions are found to exhibit both jump discontinuities and infinities, so an integral of the distributions over small intervals around various positions across the channel is introduced. Finally, the technique is applied to a

typical case of channeling of 1-MeV helium ions along the {110} planes of silicon.

II. GOVERNING EQUATIONS OF MOTION

Consider the motion of an ion channeled between two crystal planes as shown in Fig. 1. If the continuum approximation is assumed to be valid, then the s component of velocity v_0 is constant and the motion of the ion is governed by the differential equation

$$\frac{d^2x}{ds^2} = -\frac{1}{2E}\frac{dV(x)}{dx}\,, \tag{1}$$

where

$$V(x) = V_1(b+x) + V_1(b-x)\,, \tag{2}$$

$$V_1(y) = (Nd_p)\int_0^\infty 2\pi r\, U(R)\, dr\,, \tag{3}$$

$E = mv_0^2/2$, m is the mass, $2b = d_p$ is the distance between planes, $V_1(y)$ is the continuum potential for a plane at a distance y from the plane, $R = (r^2 + y^2)^{1/2}$, r is the polar coordinate in the plane, Nd_p is the number of atoms per unit area in the plane, and U is the interaction potential between an ion and a lattice atom. The derivation of the continuum approximation requires that $E = \frac{1}{2}mv_0^2$ be very close to the total energy; in our numerical calculations we take E to be the total energy. In Eq. (2) it is assumed that the continuum potential between major crystal planes is well approximated by including only the contributions from the two adjacent planes. The derivation of Eq. (3) can be found in Datz *et al.*[14] and Ellison.[15] If we write (1) as a system and make the change of variables

$$S = s/s_0, \qquad X = x/b\,,$$

$$Y = \frac{dx}{dt}\Big/\left(\frac{2K}{m}\right)^{1/2} = \left(\frac{E}{K}\right)^{1/2}\frac{dx}{ds}\,, \tag{4}$$

$$V(x) = KW(X)\,,$$

where s_0 is a characteristic distance parameter and K is a measure of the size of the potential, then the governing equations of motion in nondimensional form are

$$\begin{aligned} &\frac{dX}{dS} = \epsilon Y\,, \qquad X(0) = X_0\\ &\frac{dY}{dS} = -\tfrac{1}{2}\epsilon W'(X), \qquad Y(0) = Y_0\,, \end{aligned} \tag{5}$$

where the prime notation denotes differentiation with respect to X and

$$\epsilon = (s_0/b)(K/E)^{1/2}\,. \tag{6}$$

Consider the atomic potential

$$U(R) = (z_1z_2e^2/R)[1 - R/(R^2 + c^2a^2)^{1/2}], \tag{7}$$

due to Lindhard.[1] Then Eqs. (2)–(4) yield

$$V_1(y) = K_1[(y^2 + c^2a^2)^{1/2} - y] \tag{8}$$

and

$$\begin{aligned} V(x) &= K_1\{[(b+x)^2 + c^2a^2]^{1/2}\\ &\quad + [(b-x)^2 + c^2a^2]^{1/2} - 2b\}\,, \end{aligned} \tag{9}$$

$$V(x) = K_1b\{[(1+X)^2 + D]^{1/2} + [(1-X)^2 + D]^{1/2} - 2\}\,,$$

where $D = c^2a^2/b^2$ and $K_1 = 2\pi z_1z_2e^2(Nd_p)$. Here z_1 and z_2 are the atomic number of the projectile and lattice atoms, respectively, a is the Thomas-Fermi screening distance, and c is a constant of the potential ($c \approx \sqrt{3}$). The choice of K in Eq. (4) is somewhat arbitrary, since the only requirement is that $W'(X)$ be of order one. We choose

$$K = K_1b = 2\pi z_1z_2e^2(Nd_p)\,b\,, \tag{10}$$

therefore,

$$W(X) = [(1+X)^2 + D]^{1/2} + [(1-X)^2 + D]^{1/2} - 2\,. \tag{11}$$

A commonly used quantity in discussions of planar channeling is

$$\varphi_r = [2\pi z_1z_2e^2(Nd_p)\,a/E]^{1/2}\,.$$

For example, it is commonly assumed that the critical angle is $\beta\varphi_r$ where β is an order-one quantity.[9,16] ϵ and Y can be written in terms of φ_r as

$$\epsilon = (s_0^2/ab)^{1/2}\,\varphi_r\,, \tag{12}$$

$$Y = \left(\frac{a}{b}\right)^{1/2}\frac{dx}{ds}\Big/\,\varphi_r\,. \tag{13}$$

If s_0^2 is picked of the order ab, then ϵ is the order of magnitude of φ_r. If $\varphi(s)$ is the angle a trajectory makes with the planes then

$$\frac{dx}{ds} = \tan\varphi(s)\,.$$

For channeling φ is small and $\tan\varphi$ is approximately φ, therefore,

$$Y \approx (a/b)^{1/2}\,(\varphi/\varphi_r)\,. \tag{14}$$

The perfect plane model for channeling assumes the applicability of Newtonian mechanics with each lattice atom characterized by a screened coulomb potential, and ignores thermal effects (vibration of the lattice atoms) and electronic effects which are

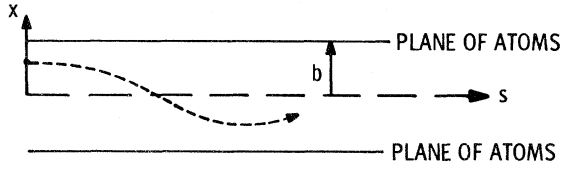

FIG. 1. Schematic of a channeled trajectory between a pair of crystal planes.

not included in a screened coulomb potential. The continuum plane model [Eqs. (1)–(6)] is an approximation to this model which smooths out the effect of the individual atoms and thereby considerably simplifies the equations. The method of averaging of Krylov and Bogoliubov[17] has been used to obtain error bounds relating these two models[15]; the errors go to zero as $\epsilon \sim \varphi_r \to 0$. So, a necessary condition for the validity of the continuum model is that ϵ be a small parameter.

Notice that (5) are the equations of motion for a nonlinear oscillator and have an associated conservation law,

$$E_\perp(X, Y) = Y^2 + W(X) = E_{\perp 0}, \tag{15}$$

where the initial conditions in (5) infer that $E_{\perp 0} = Y_0^2 + W(X_0)$. This is simply a normalized form of the transverse energy which is frequency used in continuum model estimates.

There are a variety of planar continuum potentials that have been used in channeling calculations, based, for example, on atomic potential forms of Lindhard [see Eq. (7)], Bohr, and Moliere.[3] For each of these, the solutions of (5) are periodic with period P depending on $E_{\perp 0}$. In fact for these potentials the oscillator (5) behaves like a hard spring (as opposed to the pendulum equation which behaves like a soft spring), that is,

$$\frac{dP}{dE_{\perp 0}} < 0.$$

For each energy $E_{\perp 0} > W(0)$, Eq. (15) defines a curve in the X-Y plane. Each of these curves is called an *integral curve* of Eqs. (5) and the X-Y plane is referred to as the *phase plane*. If one of the planar continuum potentials is used, the integral curves form a family of concentric ovals about the origin.

Consider the motion of a channeled ion as defined by (5). The initial conditions given in (5) determine the ion's energy $E_{\perp 0}$, which in turn defines an integral curve in the phase plane according to (15). Because of conservation of energy, the X, Y position of the ion in the phase plane moves in a clockwise direction around the integral curve as the ion physically moves through the crystal. The ion's motion is periodic and it returns to its initial position (X_0, Y_0) in phase plane after a period which depends on $E_{\perp 0}$.

If we consider Lindhard's planar continuum potential and channeling with 1-MeV helium ions along the {110} plane of silicon at room temperature, then $W(X)$ is given in Eq. (11),

$$\epsilon = 0.015\,272, \tag{16}$$

$$D = 0.0965, \tag{17}$$

where we have taken $s_0 = 1$ Å. Let A be the amplitude of the oscillation, then the period, in angstroms, as a function of amplitude is shown in Fig. 2 [notice that $E_{\perp 0} = W(A)$]. It is a simple calculation to find $P(A)$ at $A = 0$ by linearizing $W'(X)$ about the only equilibrium point $X = 0$; the other values of P were found by integrating Eqs. (5) numerically with $X_0 = A$ and $Y_0 = 0$.

III. CALCULATION OF DISTRIBUTIONS

Consider an ion beam entering a perfect crystal in such a way that the beam is aligned with a low index crystal plane. Physically we know the ion beam is much less dense than the crystal; also we are only interested in the relative position of the ions in the various channels, and we assume all the channels in a given crystal direction are the same. Therefore, for mathematical purposes, we can take the view that all ions enter between two adjacent atomic planes with a uniform spatial distribution, with no ion-ion interaction. The problem is to find the spatial and velocity distribution of the channeled particles as they move through the crystal given their initial distribution. Because of the large number of particles involved and because their trajectories do not have simple analytic representations, most researchers have assumed statistical equilibrium in their calculations.[2,3,18] However, an examination of the motion in the phase plane (*phase flow*) leads to a convenient way to order the ions and further study leads to two very simple quantities, described by a system of differential equations, from which the distributions can be computed. The continuum approximation is used but no assumption of statistical equilibrium is required in this approach.

We shall describe a method for calculating the evolution of the spatial distribution and various integrals of it for a perfectly aligned beam with uniform distribution initially. It is easy to modify this method for nonuniform initial distributions and nonzero incident angles. It will also be clear

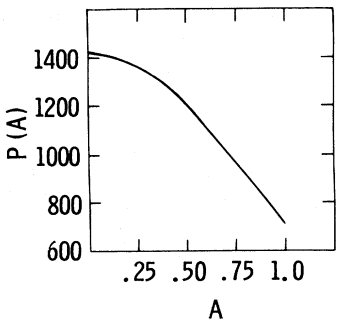

FIG. 2. Period in angstroms vs nondimensional amplitude for the solutions of Eqs. (5) with Lindhard's standard potential for 1-MeV helium ions channeled along the {110} planes of silicon. Amplitude in angstroms is bA where $b = 0.96$ Å.

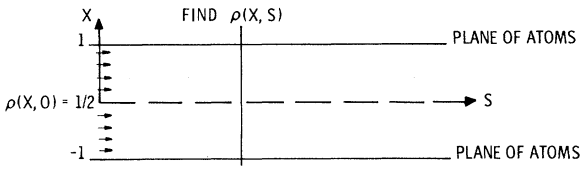

FIG. 3. Schematic of the calculational goal to find the spatial distribution ρ at a depth S into the crystal given a uniform initial distribution.

how to calculate the velocity distribution and related integrals.

Let $\rho(X, S)$ denote the spatial distribution of the ions at a distance S into the crystal. As indicated in Fig. 3, the problem is to find $\rho(X, S)$ given $\rho(X, 0)$. For convenience we take $\rho(X, 0) = \frac{1}{2}$; then the total "mass" between $X = \pm 1$ is 1, and ρ gives the spatial probability density. The first step in finding the spatial distribution is to find a convenient way to order the ions. The differential equations governing the motion of the ions are given by (5) with $Y_0 = 0$:

$$\frac{dX}{dS} = \epsilon Y, \qquad X(0, X_0) = X_0,$$
$$\frac{dY}{dS} = -\tfrac{1}{2}\epsilon W'(X), \qquad Y(0, X_0) = 0, \tag{18}$$

where $X = X(S, X_0)$ and $Y = Y(S, X_0)$.

In the phase plane, the initial positions of the particles are uniformly distributed along the line $Y = 0$, $X \in [-1, 1]$; see curve a in Fig. 4. For this case we need only consider those particles starting with $X \in [0, 1]$ because of the symmetry. However, in the treatment of the nonaligned case where $Y_0 \neq 0$ this symmetry is lost, and so here we describe a method for finding the distribution that is easily adaptable to the uniform nonaligned case. If we integrate the differential equations (18) for various $X_0 \in [-1, 1]$ from $S = 0$ to some S we obtain the functions $X(S, X_0)$ and $Y(S, X_0)$. These functions

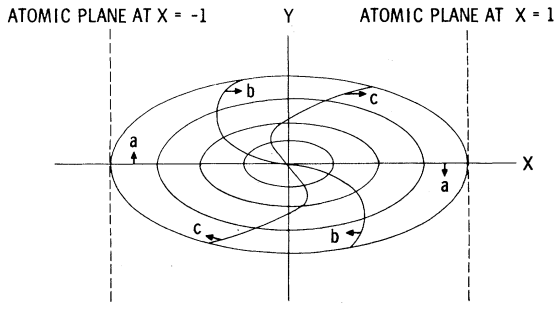

FIG. 4. Phase flow in the phase plane for Eqs. (18). Curve a represents the initial positions and velocities of the ions; curves b and c represent the positions and velocities of the ions at two different depths into the crystal. Ovals are integral curves.

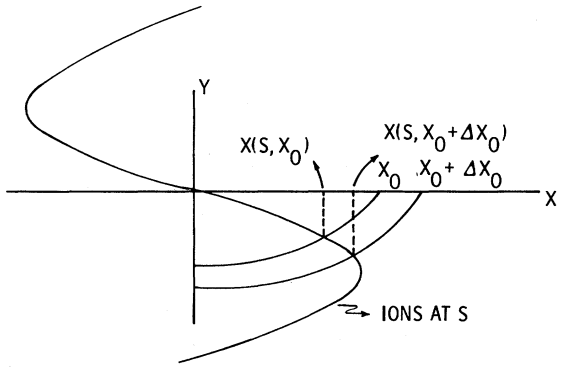

FIG. 5. Geometrical interpretation of the use of a phase flow curve to calculate the contribution to the spatial distribution near $X(S, X_0)$ due to those particles which started near X_0.

can be interpreted in two ways: (i) they give the parametric representation of an integral curve in the phase plane if S is allowed to vary and X_0 is held fixed (see the oval curves in Fig. 4), and (ii) they give the parametric representation of the b and c type curves in Fig. 4 if X_0 is allowed to vary and S is held fixed. The b- and c-type curves give the position and velocity of each ion in the channel for various depths into the crystal; these are called the phase flow for curve a. Notice that the hard-spring effect shows up in the phase flow in that those ions on the outer integral curves have a larger rate of angular movement around the phase plane than those starting on the inner ones. As S increases these curves wrap themselves around the origin.

The next step is to determine how to obtain the spatial and velocity distributions from the phase flow. Observe that as a consequence of conservation of transverse energy [Eq. (15)] the ions which start between two integral curves remain between them. Let us take a closer look at a typical curve like b or c and consider two integral curves defined by X_0 and $X_0 + \Delta X_0$, as shown in Fig. 5. The key idea here is that those ions which start in $[X_0, X_0 + \Delta X_0]$ are located in the X interval $[X(S, X_0), X(S, X_0 + \Delta X_0)]$ at a distance S into the crystal. Given S and X_0, let $\mu(S, X_0)$ denote the spatial distribution at $X(S, X_0)$ due to those ions starting "near" X_0. Thus we have the approximate relation

$$\mu(S, X_0)\left(\left| X(S, X_0 + \Delta X_0) - X(S, X_0)\right|\right) \approx \tfrac{1}{2}\Delta X_0 . \tag{19}$$

In the limit as $\Delta X_0 \to 0$ Eq. (19) leads to

$$\mu(S, X_0) = \left(2\left|\frac{\partial X(S, X_0)}{\partial X_0}\right|\right)^{-1} . \tag{20}$$

To find $\rho(X, S)$ for fixed S, we must find all the X_0's corresponding to a given position X (notice that in the example shown in Fig. 5 there are two). This requires solution of the nonlinear equation

$$X(S, X_0) - X = 0 . \tag{21}$$

The spatial distribution at X is then given by

$$\rho(X, S) = \sum \mu(S, X_0) , \tag{22}$$

where the sum is taken over all X_0 such that $X - X(S, X_0) = 0$.

One could calculate $\mu(S, X_0)$ approximately from Eq. (19), however, there is a more convenient way since $\partial X/\partial X_0$ satisfies the variational equations for (18). Let

$$p(S, X_0) = \frac{\partial X(S, X_0)}{\partial X_0} ,$$
$$q(S, X_0) = \frac{\partial Y(S, X_0)}{\partial X_0} , \tag{23}$$

then $p(S, X_0)$ can be determined from the following equations:

$$\begin{aligned} &\frac{dX}{ds} = \epsilon Y, && X(0, X_0) = X_0 \\ &\frac{dY}{dS} = -\tfrac{1}{2}\epsilon W'(X), && Y(0, X_0) = 0 \\ &\frac{dp}{dS} = \epsilon q, && p(0, X_0) = 1 \\ &\frac{dq}{dS} = -\tfrac{1}{2}\epsilon W''(X) p, && q(0, X_0) = 0, \end{aligned} \tag{24}$$

where $W''(X)$ is the second derivative of $W(X)$ with respect to X.

Notice that the spatial distribution becomes unbounded at points $X = X(S, X_0)$ where $p(S, X_0) = 0$ (see points of vertical slope on curves b and c of Fig. 4); that the number of these infinities becomes countably infinite as $S \to \infty$; and that the distribution has jump discontinuities at $X = X(S, \pm 1)$. The velocity distribution can be discussed in a similar manner by considering $q(S, X_0)$. If the initial distribution is nonuniform, this distribution in X_0 will replace the $\frac{1}{2}$ in Eq. (19).

If the oscillator in Eq. (18) is linear, that is,

$$W'(X) = 2\beta^2 X , \tag{25}$$

where β is some constant, then the distribution can be computed analytically. Solving Eqs. (24) and noticing that curves b and c in Fig. 4 become straight lines we find

$$\rho(X, S) = \begin{cases} 1/2a & \text{for } |X| \le a , \\ 0 & \text{for } a < |X| \le 1 , \end{cases} \tag{26}$$

where $a = |\cos \epsilon \beta S|$. For more realistic potentials the problem has to be tackled numerically.

An algorithm has been constructed for computing the distribution on an IBM 360 using a double precision version of a differential equation solver called RKF which was developed by Allen and Shampine and is discussed in their book.[19] This code integrates a system of first-order ordinary differential equations by a fourth-order Runge-Kutta method and uses fifth-order Runge-Kutta formulas to automatically estimate the local error and adjust the step size. We present the algorithm here not only so that those interested can duplicate the results but also because an understanding of the algorithm yields a more complete understanding of the structure of the distribution. The algorithm performs as follows: (a) It numerically integrates the differential equations (24) with $X_0 = \pm 0.005n$, $n = 0, 1, 2, \ldots, 200$ from $S = 0$ to S; this is done all at once, using RKF, by writing Eqs. (24) as a system of 1604 equations. (For the examples discussed in Sec. IV we found dividing the X_0 interval into 400 subintervals to be satisfactory.) (b) It prints out $X(S, 1)$ and $X(S, -1)$ ($n = 200$ and $n = -200$) for the location of the jump discontinuities in $\rho(X, S)$. (c) It uses linear interpolation on the data computed in (a) to find the X_0's where $p(S, X_0)$ is zero; these give the points $X = X(S, X_0)$ (use linear interpolation again) where $\rho(X, S)$ becomes unbounded. (d) It calculates the $\max X(S, X_0)$ and the $\min X(S, X_0)$ over $X_0 \in [-1, 1]$ from the data in (a), thus giving the points X where $\rho(X, S)$ drops to zero. (e) It finds $\rho(X, S)$ by picking a value of $X \in [X_{\min}, X_{\max}]$ and then using linear interpolation to find all the X_0's such that $X - X(S, X_0) = 0$, and to find $p(S, X_0)$ for each of these X_0's. The sum in Eq. (22) is then computed to obtain $\rho(X, S)$.

A simple modification of this algorithm allows calculations for nonuniform initial distributions and ion beams at nonzero angles with respect to the planes.

Since the distribution function $\rho(X, S)$ exhibits both jump discontinuities and infinities, we felt it would be interesting to examine integrals $M(I, S)$ of $\rho(X, S)$ over various intervals $I = \{X \mid a \le X \le b\}$, that is,

$$M(I, S) = \int_a^b \rho(\xi, S)\, d\xi .$$

The quantity $100M(I, S)$ has the obvious physical interpretation of being the percentage of particles in the interval I at a distance S into the crystal and is perhaps a more interesting quantity than ρ for applications of channeling such as lattice-site location studies. At first glance one might consider computing the integral of ρ directly, however, there is a much simpler approach, an approach which is simpler than finding $\rho(X, S)$. A study of Fig. 5 and Eqs. (19)–(22) shows that the contribution to $M(I, S)$, where $I = [X(S, X_0), X(S, X_0 + \Delta X_0)]$, due to the particles starting in $[X_0, X_0 + \Delta X_0]$, is $\frac{1}{2}\Delta X_0$. To find $M(I, S)$ we must find all the X_0 intervals which contribute particles to I, add up to the length

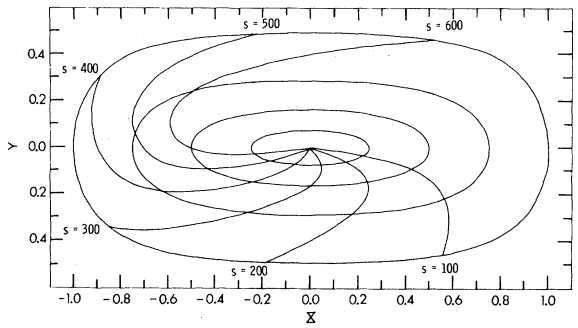

FIG. 6. Phase flow at various crystal depths (in angstroms) for a perfectly aligned 1-MeV beam of helium ions channeled along the {110} planes of silicon. Integral curves (ovals) correspond to $E_{\perp 0} = W(0.25)$, $W(0.5)$, $W(0.75)$, and $W(1)$.

of these intervals, and multiply by $\frac{1}{2}$. In the case shown in Fig. 5 there are two X_0 intervals which contribute particles to I.

More formally then, to calculate $M(I, S)$, $I=[a, b]$, we must find all the X_0's corresponding to a and b at a depth S into the crystal. That is, solve the equations

$$X(S, X_0) - a = 0$$

and

$$X(S, X_0) - b = 0.$$

This gives all the X_0 intervals which contribute particles to I at a distance S into the crystal. Summing the lengths of these intervals and multiplying by $\frac{1}{2}$ gives $M(I, S)$. An algorithm has been written to do this and the results in a specific case will be illustrated in the next section. In developing this algorithm it was found helpful to study both the phase flow and the graph of $X(S, X_0)$ vs X_0 for S fixed.

IV. APPLICATION

In this section we consider the channeling of 1-MeV helium ions along the {110} planes of silicon not only for its intrinsic interest but also because it gives more insight into the ideas of Sec. III. We present (i) the spatial distribution at various depths into the crystal for a perfectly aligned ion beam which is uniformly distributed initially, (ii) various integrals of this distribution, and (iii) the spatial distribution for a uniformly distributed ion beam entering the crystal at a nonzero angle with respect to the {110} plane. The calculations are done with Lindhard's standard potential with $s_0 = 1$ Å, so that S represents the distance into crystal in angstroms. The potential and the two parameters in this case are

$$W(X; D) = [(1+X)^2 + D]^{1/2} + [(1-X)^2 + D]^{1/2} - 2,$$

$$\epsilon = 0.015\,27, \qquad (27)$$

$$D = 0.0965.$$

Actually the curves presented here are valid for arbitrary $\epsilon > 0$ as can be seen by considering the initial value problem

$$\frac{dZ}{dt} = \epsilon f(Z), \qquad Z(0) = Z_0, \qquad (28)$$

which defines a vector function $Z(t; \epsilon)$, and has the form of both Eqs. (5) and (24). It is easy to verify that $Z(S; \epsilon_0) = Z((\epsilon_0/\epsilon)S; \epsilon)$ for every $S \geq 0$; therefore if a certain phenomenon occurs at a distance S_0 into the crystal for $\epsilon = \epsilon_0$ then it occurs at a distance $(\epsilon_0/\epsilon)S_0$ into the crystal for arbitrary ϵ. For example, $\rho(X, S_0; \epsilon_0) = \rho(X, (\epsilon_0/\epsilon)S_0; \epsilon)$ and $M(I, S_0; \epsilon_0) = M(I, (\epsilon_0/\epsilon)S_0; \epsilon)$. It should be noted that the value of D, which depends on the ratio of a to b, must remain fixed. So, for example, the curves we present are valid for a large range of ion beam energies, E, but are not valid for other planar spacings unless there is a corresponding change in the screening distance, a.

Consider the evolution of a perfectly aligned 1-MeV beam of helium ions uniformly distributed as it enters the {110} planes of a silicon crystal. The phase flow is shown in Fig. 6 for various distances into the crystal for those particles entering the channel in the interval $X \in [0, 1]$. The phase flow for those particles starting in $[-1, 0]$ is obtained by rotating the curves by 180° (see Fig. 4).

This figure not only gives an over-all picture of what is happening but it gives considerable information about the structure of ρ, such as, the X region where it is zero, the position of the jump discontinuities, the positions where it becomes unbounded, and the initial positions of the particles which contribute to the distribution at some given position X. As an example consider the phase flow curve for $S = 200$, including the portion due to those particles starting in $[-1, 0]$. It has vertical slopes at $|X| = \gamma_1$ where $\gamma_1 \approx 0.25$ and no portion of the curve lies in the region of the phase plane defined by $|X| > \gamma_1$. Therefore the spatial distribution becomes unbounded as $|X| \to \gamma_1$ from below and is zero for $\gamma_1 < |X| \leq 1$. The integral curve which goes through $X = 0.5$, $Y = 0$ comes close to crossing the phase flow curve near its vertical slopes; interpolation indicates that the initial positions of those particles contributing to the infinities at $X = \pm\gamma_1$ are near $X_0 = \pm 0.55$, respectively. The jump discontinuities occur at the X position where the phase flow curve meets the outer integral curve (i.e., the integral curve which goes through the point $X = 1$, $Y = 0$); this happens at $|X| \approx 0.18$. As a final observation notice that the particles contributing to the particle density at $X = 0$ come from $X_0 = 0$ and $|X_0| \approx 0.87$. If one is interested only in

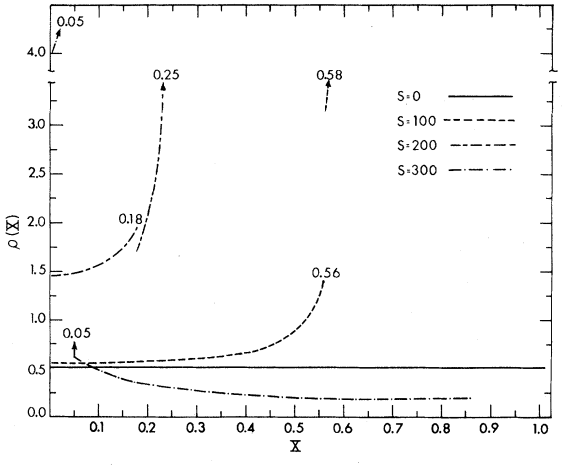

FIG. 7. Spatial distribution at depths of 0, 100, 200, and 300 Å for a perfectly aligned 1-MeV beam of helium ions, uniformly distributed initially, channeled along the {110} planes of silicon. Positions of the jump discontinuities and infinities are marked; ρ is given only for the $X \geq 0$ since it is symmetric about the center of the channel.

the spatial distribution another interesting set of curves is $X(S, X_0)$ vs X_0 for various S.

The spatial distribution curves corresponding to Fig. 6 are presented in Figs. 7 and 8 for $X \geq 0$ since $\rho(X, S) = \rho(-X, S)$; compare the distribution for $S = 200$ in Fig. 7 with the comments in the previous paragraph. A study of the distributions indicates a predominant flux peak at the center of the channel ($X = 0$) at a depth of about $S = 300$. This is also indicated by the phase flow curves, as flux peaking is to be expected near $X = 0$ when the vertical slopes on the phase flow curves are near $X = 0$. However, the clearest picture of the flux peaking is found by a study of $M([-0.05, 0.05], S)$.

In Fig. 9 we present plots of $M_i(S) = M(I_i, S)$ vs S for $I_1 = [-0.05, 0.05]$, $I_2 = [0.15, 0.25]$, $I_3 = [0.45, 0.55]$, and $I_4 = [0.75, 0.85]$. Notice the flux peaking phenomenon and the "damping" of the oscillations as S increases. The phase flow curves are again useful for interpreting Fig. 9, for example: (a)

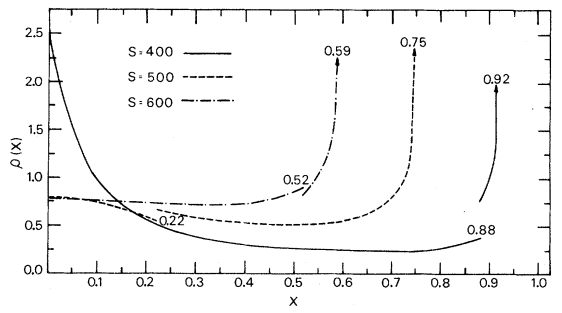

FIG. 8. As in Fig. 7 for depths of 400, 500, and 600 Å.

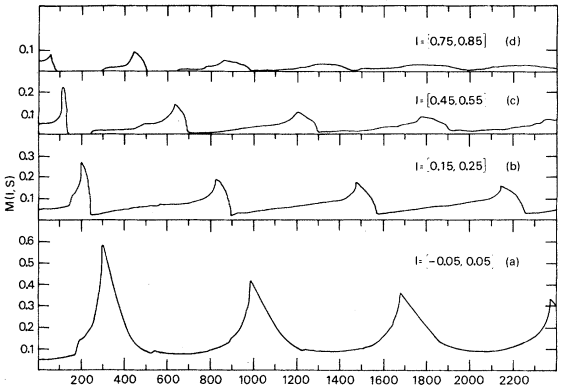

FIG. 9. Variation of $M(I, S)$ with depth (angstroms) for the case treated in Figs. 7 and 8. (a) $I = [-0.05, 0.05]$; (b) $I = [0.15, 0.25]$; (c) $I = [0.45, 0.55]$; (d) $I = [0.75, 0.85]$.

The first flux peak for M_1, M_2, and M_3 occurs when the vertical slope on the phase flow curve first enters the intervals I_1, I_2, and I_3, respectively. The initial position of the particles contributing to the rapid rise in M near the flux peaks can be found approximately. We discuss this for $M_1(S)$. (b) The phase flow curve for $S = 300$ shows that the first flux peak in M_1 is made up of those particles which started with $|X_0| \leq \gamma_2$, where $\gamma_2 \approx 0.58$, since the portion of the curve which corresponds to those particles is contained in I_1. The rapid increase in $M_1(S)$ near the flux peak occurs when the vertical slope on the phase flow curve enters I_1. By interpolation we estimate that the integral curve through $X = 0.3$, $Y = 0$ goes through the vertical slope on the $S = 300$ phase flow curve. We conclude that the particles contributing to the rapid rise in $M_1(S)$ near $S = 300$ started near $|X_0| = 0.3$. (c) The sharp increase in $M_1(S)$ near $S = 175$ is due to the particles which started near the planes entering the interval I_1 for the first time, and the small increase near $S = 550$ is due to the same particles entering I_1 for the second time.

There seems to be considerable speculation in the literature concerning the location of the first flux peak near the center of the channel. An argument by Gemmel[2] (p. 156) based on the oscillation in minimum yield calculations by Barrett[9] indicates that the first flux peak in planar channeling should occur near $S = \frac{1}{4}\lambda_{ch}$, where λ_{ch} is the period of oscillation for those particles starting near the planes. It can be seen from Fig. 2 that this gives an estimate which is low compared to the $S = 300$ found for $M_1(S)$. One reason for the difference is that the particles which cause the rapid rise in $M_1(S)$ near the first flux peak started near $X_0 = \pm 0.3$, whereas those particles which most strongly affect minimum-yield oscillations start near the planes. Another possible source of difference is that the Monte Carlo calculations of Barrett include

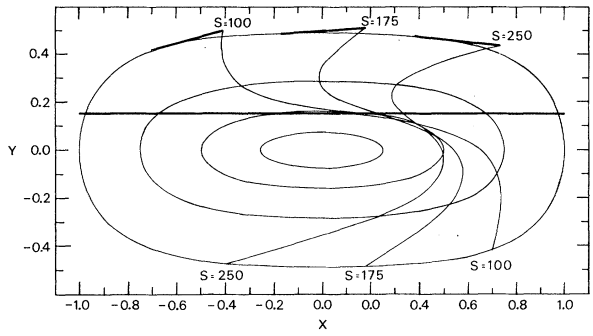

FIG. 10. Phase flow at various crystal depths for a nonaligned 1-MeV beam of helium ions channeled along the {110} planes of silicon. Initial phase flow curve ($S=0$) is the straight line given by $Y=0.1539$, $-1\leq X\leq 1$. Integral curves are as in Fig. 6.

thermal vibration of the lattice atoms whereas our results do not.

We are currently studying $M(I, S)$ for large S to gain a better understanding of questions concerning the approach of the particle spatial distribution to statistical equilibrium. Because of the jump discontinuities and infinities in ρ it seems that some smoothing has to be done in order to consider such questions and a study of $M(I, S)$ seems like one reasonable approach. $M(I, S)$ has been computed for relatively large S and it appears to approach a limit[20]; however, it is not clear how accurate the calculations are for this range of S, and, of course, the existence of a limit can only be hinted at with the aid of a computer. We plan to compare the behavior of $M(I, S)$ for large S with the corresponding integrals of the statistical equilibrium distribution.

As a final example we consider the evolution of the spatial distribution for a uniform ion beam entering the crystal at a nonzero angle. This has the consequence that particles starting near the planes will eventually penetrate the planes; these particles need special consideration. For numerical purposes we choose

$$Y(0, X_0)=[W(1)-W(0.975)]^{1/2}\approx 0.1539\equiv Y_0 . \quad (29)$$

Thus those particles which start with $\alpha\equiv 0.975 \leq |X_0|\leq 1$ eventually penetrate the plane. The value of Y_0 in Eq. (29) corresponds to an angle of approximately 0.128°. The measured half-angle for 1-MeV helium ions along the {110} planes of silicon is $0.22°\pm 0.03°$.[16]

To maintain the spirit of the calculation we assume that when a particle trajectory reaches $X=1$ it is instantaneously transported across the channel to $X=-1$ with its energy $E_\perp$ conserved (since $X=1+\delta$ is energetically equivalent to $X=-1+\delta$). Physically, this assumes that the particle moves through the plane with no change in angle. This is a realistic assumption since computer simulation calculations by Barret (in particular Fig. 5 of Ref. 9 and damage rate versus depth calculations for various incident angles[21]) and experimental results by van der Weg, Roosendaal and Kool[4] indicate that a significant number of particles do penetrate the planes and continue a governed rather than random motion.

Figure 10 is the phase flow plot of the particles calculated for $S=100$, 175, and 250; the initial particle positions lie on the line $Y=Y_0$, $X\in[-1, 1]$. Notice that the particles starting in $[-0.25, 0.25]$ have nearly the same energy, that is, they all lie nearly on the same integral curve. Also notice that the particles which start in $[-1, -\alpha]\cup[\alpha, 1]$ lie outside the integral curve which goes through $X=1$, $Y=0$, and will therefore remain outside as a consequence of conservation of energy. At the particular depths considered in the figure the particles which started in $[-1, -\alpha]$ have not penetrated the planes whereas those which started in $[\alpha, 1]$ have penetrated just once. If $X(S, X_0)$, $Y(S, X_0)$, $p(S, X_0)$ and $q(S, X_0)$ denote the functions defined by Eq. (24), with the modification, $Y(0, X_0)=Y_0$, then the phase flow curves for the particles which start in $[-1, \alpha]$ are given by $X(S, X_0)$, $Y(S, X_0)$, with S fixed.

The phase flow curves for the particles which start in $[\alpha, 1]$ must be calculated separately. Let $X_0=\xi$ be the initial position of one of these particles and let $d(\xi)$ be the distance S traveled by this particle as it moves from $X=\xi$ to $X=1$. The phase plane position of this particle for the range of S considered is given by

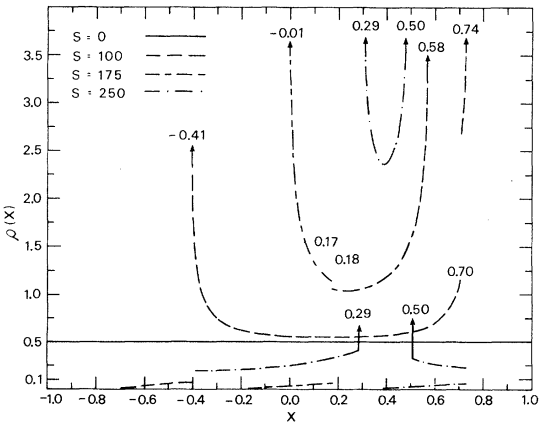

FIG. 11. Spatial distribution at depths of 0, 100, 175, and 250 Å for a nonaligned beam of 1-MeV helium ions, uniformly distributed initially, channeled along the {110} planes of silicon. Curves with ρ less than 0.1 give the distribution of those particles which have penetrated the planes; Other curves give the distribution of the rest of the particles. Total distribution is just the sum of the two contributions. Positions of the jump discontinuities and infinities are marked.

$$X = X(S', -\xi), \qquad Y = Y(S', -\xi), \tag{30}$$

where $S' = S - 2d(\xi)$, as can be checked by noting that these functions satisfy the differential equations in Eq. (24) with initial conditions $X = X(-d(\xi), -\xi) = -1$ and $Y = Y(-d(\xi), -\xi) = Y(d(\xi), \xi)$ at $S = d(\xi)$. Equations (30), considered as functions of $\xi \in [\alpha, 1]$ with S fixed, give the phase flow of the particles which have penetrated the plane. The long tail at the upper end of each phase flow curve is the phase flow for these particles. It is interesting to note that the length of these tails does not vary much for $100 \leq X \leq 250$; the length is determined primarily by the variation of $d(\xi)$, $\xi \in [\alpha, 1]$.

The contribution to the spatial distribution from the particles starting in $[-1, \alpha]$ is computed just as in the perfectly aligned case with the exception that $Y(0, X_0) = Y_0$ in Eqs. (24). The contribution from the other particles can be computed as suggested in Eqs. (20)–(24) using Eqs. (30) and noting that

$$\frac{\partial X(S', -\xi)}{\partial \xi} = -2\epsilon d'(\xi)\, Y(S', -\xi) - p(S', -\xi). \tag{31}$$

However, for the range of S considered the distribution can be computed just as accurately as suggested by Eq. (19), and we used this latter method in our numerical calculations.

The calculated spatial distributions due to those particles with $-1 \leq X_0 \leq \alpha$ and with $\alpha \leq X_0 \leq 1$ are presented separately in Fig. 11 since the contribution from the particles which have penetrated the plane is so small (for the particular case considered this contribution, for each S, is less than 0.1). The total spatial distribution is just the sum of the two contributions.

ACKNOWLEDGMENTS

My thanks to S. T. Picraux, D. K. Brice, W. T. Kyner, and J. Starner for many helpful discussions and to Sandia Laboratories for partial support of this work under a Sandia/UNM grant.

[1] J. Lindhard, K. Dan. Vidensk. Selsk. Mat.-Fys. Medd. 34, No. 14 (1965).
[2] D. S. Gemmell, Rev. Mod. Phys. 46, 129 (1974).
[3] D. V. Morgan, *Channeling* (Wiley, New York, 1973).
[4] F. Abel, G. Amsel, M. Bruneaux, and C. Cohen, U. S.-Italy Seminar on Ion-Beam Analysis, Catania, Italy, June 1974 (unpublished); W. F. van der Weg, H. E. Roosendaal, and W. H. Kool, Radiat. Eff. 17, 91 (1973).
[5] F. Eisen and E. Uggerhøj, Radiat. Eff. 12, 233 (1972).
[6] S. T. Picraus, in *New Uses of Low-Energy Accelerators*, edited by J. F. Ziegler (Plenum, New York, to be published).
[7] S. T. Picraux, W. L. Brown, and W. M. Gibson, Phys. Rev. B 6, 1382 (1972).
[8] J. A. Davies in Ref. 3, p. 391.
[9] J. H. Barrett, Phys. Rev. B 3, 1527 (1971).
[10] J. H. Barrett, Phys. Rev. Lett. 31, 1542 (1973).
[11] D. Van Vliet, Radiat. Eff. 10, 137 (1971).
[12] D. V. Morgan and D. Van Vliet, Radiat. Eff. 12, 203 (1972).
[13] D. V. Morgan in Ref. 3, p. 79.
[14] S. Datz, C. Erginsoy, G. Leibfried, and H. L. Lutz, Annu. Rev. Nucl. Sci. 17, 129 (1967).
[15] J. A. Ellison, University of New Mexico Mathematics Department technical report, 1974 (unpublished).
[16] S. T. Picraux, Air Force Cambridge Research Laboratories scientific report, 1969 (unpublished).
[17] N. N. Bogoliubov and Y. A. Mitropolsky, *Asymptotic Methods in the Theory of Nonlinear Oscillations* (Gordon and Breach, New York, 1961).
[18] E. Bonderup, H. Esbensen, J. U. Anderson, and H. E. Schiott, Radiat. Eff. 12, 261 (1972).
[19] L. F. Shampine and R. C. Allen, *Numerical Computing: An Introduction* (Saunders, Philadelphia, 1973).
[20] If the oscillator is linear then $M(I, S)$ can be found exactly from Eq. (26). In this case M is a periodic function of S and therefore will not approach a limit as $S \to \infty$. The reason for this is that all the particles have the same period. If $M(I, S)$ approaches a limit for large S in the case of a nonlinear oscillator it will be due to the spread in periods of the various particles.
[21] J. H. Barrett (private communication).